ACS Photonics

Article

pubs.acs.org/journal/apchd5

Link between Cathodoluminescence and Electron Energy Loss Spectroscopy and the Radiative and Full Electromagnetic Local Density of States

Arthur Losquin*,† and Mathieu Kociak‡

†Department of Physics, Lund University, P.O. Box 118, SE-221 00 Lund, Sweden

‡Laboratoire de Physique des Solides CNRS/UMR8502, Bâtiment 510, University Paris-Sud, Orsay 91405, France

Supporting Information

ABSTRACT: Electron energy loss spectroscopy (EELS) and cathodoluminescence (CL) have proved during the past few years to be tremendous tools to study surface plasmons in metallic nanoparticles, thanks to an extremely high spatial resolution combined with a broad spectral range. Despite their apparent close resemblance, qualitative differences between EELS and CL have been theoretically as well as experimentally pinpointed. We demonstrate that these differences are recovered when comparing the full electromagnetic local density of states (EMLDOS) and the radiative EMLDOS. Following the known relation established between EELS and the projection along the electron trajectory of the full EMLDOS, we introduce a formalism based on the Maxwell electric Green tensor to draw a link between CL and the projection along the electron trajectory of the radiative EMLDOS. We discuss in simple terms the differences between EELS (projected full EMLDOS) and CL (projected radiative EMLDOS) through modal decompositions obtained in the quasistatic approximation. Contrary to EELS, CL probes only the radiative modes. Furthermore, CL resonant line shapes may be shifted and asymmetric compared to EELS. The CL asymmetry is due to interferences in the far-field radiation from spectrally and spatially overlapping modes. Our analytical expressions are illustrated through boundary element method numerical simulations.

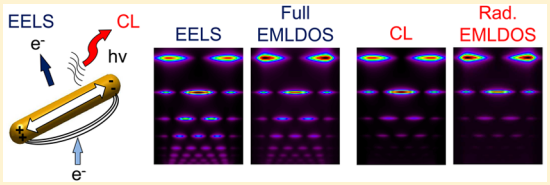

KEYWORDS: *nanooptics, plasmonics, electron energy loss spectroscopy, cathodoluminescence, electromagnetic local density of states*

The electromagnetic local density of states (EMLDOS) is a key and ubiquitous quantity in nanooptics.[1,2] For example, the EMLDOS defines the density of states of given energy locally available for the electromagnetic field[3] and provides the basis from which various macroscopic quantities can be derived, such as heat capacities or forces.[4] By analogy with the local density of states of quantum physics, the EMLDOS is also used to describe the spatial variations of the surface plasmon (SP) modes of metallic nanoparticles.[5] Finally, the EMLDOS governs the light emission properties of quantum emitters by dictating their spontaneous decay rate. In general, decay can occur through either radiative or nonradiative channels. To quantify radiative decay rates, a radiative EMLDOS, as opposed to the full EMLDOS, can be introduced. A precise knowledge of both the radiative and full EMLDOS is crucial for decay rate engineering. Different techniques can today obtain either the full EMLDOS or the radiative EMLDOS. For instance, thermal radiation scanning tunneling microscopy and illumination mode scanning near-field optical microscopy can be ideally viewed as measuring respectively the spatial variations of the full and radiative EMLDOS at constant energy.[6,7] Recently, the combined measurement of the lifetime and fluorescence intensity of fluorescent scanning probes has also provided a simultaneous access to these two quantities.[8] However, a drawback of these methods is that they allow only monochromatic measurements. Any experimental access to the spectral and spatial variations of the EMLDOS using these techniques remains currently out of sight.

Fast electron based spectroscopies analyze the interaction of fast electrons with a sample through either their energy loss (electron energy loss spectroscopy, EELS) or the subsequently emitted photons (cathodoluminescence, CL). Over the past few years, these techniques have attracted growing attention. EELS and CL allow large data sets of spectra extending from the IR to the UV to be collected with nanometer spatial resolution.[9,10] Pioneering experiments have suggested that both EELS and CL probe the spatial and spectral properties of the SP modes sustained by metallic nanoparticles.[11−14] The EMLDOS has been introduced as a theoretical support to interpret these experiments.[15,16] It has been firmly established that EELS is closely related to the projection along the electron direction of the full EMLDOS.[15,17] On the other hand, the radiative EMLDOS has been suggested as a basic quantity to which CL could be compared.[16] Nevertheless, the distinction between the full EMLDOS and the radiative EMLDOS was elusive, and CL experiments have further been theoretically related either to the EMLDOS[18,19] or to the radiative EMLDOS.[20] At present, it seems that there is no general consensus regarding which quantity CL should be compared to.

Received: July 27, 2015
Published: October 6, 2015

DOI: 10.1021/acsphotonics.5b00416
ACS Photonics 2015, 2, 1619−1627

Overall, EELS and CL experiments on metallic nanoobjects give very similar outputs.[21,22] Nevertheless, differences between EELS and CL could be anticipated over the past decade. As a simple example, analytical calculations on spheres have shown that, for small quasistatic objects, CL should probe the dipolar modes only, contrary to EELS, which also probes the multipolar modes.[23] This has been experimentally demonstrated only recently through combined EELS and CL experiments on single small nanoparticles.[24] This simple example of a difference between EELS and CL shows that a link between CL and the radiative EMLDOS, as opposed to the link between EELS and the full EMLDOS, should be firmly established.

In this article, we extend the link between EELS and the full EMLDOS to CL and the radiative EMLDOS. We introduce a general and unified formalism based on the Maxwell Green tensor to provide a clear comparison of these four quantities. We then point out differences between EELS (full EMLDOS) and CL (radiative EMLDOS) by deriving and discussing modal decompositions in the quasistatic approximation. The findings are illustrated through retarded boundary element method (BEM) numerical simulations.[25−27] This work demonstrates the great interest in performing combined EELS and CL experiments for plasmonics studies.

GENERAL THEORY

In this section, we set generally the link between the radiative EMLDOS and CL as opposed to the link between the full EMLDOS and EELS. The resemblance between the full EMLDOS and EELS on one hand and the radiative EMLDOS and CL on the other can be straightforwardly captured from classical electrodynamics definitions[2,10] (see Methods section). The full EMLDOS and EELS measure the total amount of energy transferred from an elementary excitation (monochromatic point dipole in the case of the full EMLDOS, fast electron in the case of EELS) interacting with a polarizable system, while the radiative EMLDOS and CL probe the part of this amount that is transferred to the far field. For the sake of clarity, the quantities we discuss are summarized in Table 1. We

Table 1. Discussed Quantities

abbreviation	symbol	equations	description	measurement
n-LDOS	ρ_n	1,5,13	projection along $\vec{e}_n$ of the full EMLDOS	decay rate of quantum emitter
n-rLDOS	ρ_n^{rad}	2,6,14	projection along $\vec{e}_n$ of the radiative EMLDOS	radiative decay rate
EELS	Γ^{EELS}	3,7,15	electron energy loss probability	electron energy loss spectroscopy
CL	Γ^{CL}	4,8,16	electron-induced light emission probability	cathodoluminescence

note that energy conservation dictates that, in the ideal case of a nonabsorbing system, the radiative EMLDOS is equal to the full EMLDOS and the quantities measured by CL and EELS are the same.[15] However, the systems that we consider are metallic, which is why we need to make a distinction between radiative EMLDOS (CL) and full EMLDOS (EELS).

Mathematically, the projection along the unit vector $\vec{e}_n$ of the full EMLDOS (n-LDOS) and radiative EMLDOS (n-rLDOS) at position $\vec{r}_0$ and energy $\hbar\omega_0$ can be defined[2] in Gaussian units as

$$\rho_n(\vec{r}_0, \omega_0) = \frac{1}{2\pi^2|\vec{p}_0|^2\omega_0}\Im\{\vec{p}_0^{\,*}\cdot\vec{E}_d(\vec{r}_0, \omega_0)\} \tag{1}$$

$$\rho_n^{rad}(\vec{r}_0, \omega_0) = \frac{c}{8\pi^3|\vec{p}_0|^2\omega_0^2}\int_{4\pi} d\Omega|\vec{f}_d(\Omega, \omega_0)|^2 \tag{2}$$

In these expressions, $\vec{E}_d(\vec{r}, \omega)$ and $f_d(\Omega, \omega)$ are the total electric field and far-field amplitude produced by a dipole of moment $\vec{p}_0$ and frequency ω_0 located at point $\vec{r}_0$. In the definition of the far-field amplitude, Ω denotes the direction of a vector $\vec{r}$ pointing toward infinity. It is solely defined in spherical coordinates by the combination of polar angle and azimuth angle. $d\Omega$ is the unit solid angle centered around Ω. Furthermore, the quantities measured by EELS and CL can be expressed, for a given electron trajectory $\vec{r}_e(t)$ and a given energy $\hbar\omega$, as[10]

$$\Gamma^{EELS}(\vec{r}_e(t), \omega) = \frac{e}{\pi\hbar\omega}\int dt\Re\{e^{-i\omega t}\vec{v}\cdot\vec{E}_{el}^{\,ind}(\vec{r}_e(t), \omega)\} \tag{3}$$

$$\Gamma^{CL}(\vec{r}_e(t), \omega) = \frac{c}{4\pi^2\hbar\omega}\int_{\Omega_D} d\Omega|\vec{f}_{el}^{\,ind}(\Omega, \omega)|^2 \tag{4}$$

In eqs 3 and 4, $\vec{E}_{el}^{ind}(\vec{r}, \omega)$ and $\vec{f}_{el}^{ind}(\Omega, \omega)$ denote the induced parts of the electric field and far-field amplitude produced by the fast electron, which are obtained by removing the free-space solution from the total electric field. $\vec{v}$ is the electron velocity, and Ω_D is a detection solid angle within which light is collected.

The relation between the full EMLDOS, the radiative EMLDOS, EELS, and CL can further be synthesized by introducing the electric Green tensor $\overleftrightarrow{G}(\vec{r}, \vec{r}', \omega)$ at points $\vec{r}$ and $\vec{r}'$ and frequency ω (see Methods section for details). The n-LDOS and n-rLDOS then reduce to

$$\rho_n(\vec{r}_0, \omega_0) = -\frac{2\omega_0}{\pi}\Im\{\vec{e}_n\cdot\overleftrightarrow{G}(\vec{r}_0, \vec{r}_0, \omega_0)\cdot\vec{e}_n\} \tag{5}$$

$$\rho_n^{rad}(\vec{r}_0, \omega_0) = \frac{2\omega_0^2 c}{\pi}\int_{4\pi} d\Omega\vec{e}_n\cdot[\overleftrightarrow{G}_\infty(\Omega, \vec{r}_0, \omega_0)]^T\overleftrightarrow{G}_\infty^{\,*}(\Omega, \vec{r}_0, \omega_0)\cdot\vec{e}_n \tag{6}$$

Equation 5 is well known and can also be found either from a quantum mechanical or a statistical definition of the EMLDOS.[2] In order to derive eq 6, we introduce (see Methods) the far-field asymptote of the Green tensor $\overleftrightarrow{G}_\infty(\Omega, \vec{r}', \omega)$, which depends on the direction Ω, position $\vec{r}'$, and frequency ω. Contrary to $\overleftrightarrow{G}$, $\overleftrightarrow{G}_\infty$ does not depend on the full position $\vec{r}$, as it is independent of its modulus. However, it does depend on its direction through Ω. In eq 6, $[]^T$ denotes a tensor transpose. Similarly, EELS and CL can be expressed, considering a fast electron traveling along the z axis at position $\vec{R}(\vec{r}_e(t) = \vec{R} + z(t)\vec{e}_z)$, as:

$$\Gamma^{EELS}(\vec{R}, \omega) = -\frac{4e^2}{\hbar} \times \Im\{\vec{e}_z\cdot\overleftrightarrow{G}^{ind}(\vec{R}, \vec{R}, \omega/v, -\omega/v, \omega)\cdot\vec{e}_z\} \tag{7}$$

DOI: 10.1021/acsphotonics.5b00416
ACS Photonics 2015, 2, 1619−1627

$$\Gamma^{CL}(\vec{R},\omega) = \frac{4\omega c e^2}{\hbar} \times \int_{\Omega_D} d\Omega \vec{e}_z \cdot [\overleftrightarrow{G}^{ind}_{\infty}(\Omega,\vec{R},\omega/v,\omega)]^T \times \overleftrightarrow{G}^{ind*}_{\infty}(\Omega,\vec{R},\omega/v,\omega)\cdot\vec{e}_z \quad (8)$$

In eq 7, which has been derived previously,[15] $\overleftrightarrow{G}^{ind}(\vec{R},\vec{R},k_z,k_z',\omega)$ is the Fourier transform of $\overleftrightarrow{G}^{ind}$ with respect to z and z'. In eq 8, $\overleftrightarrow{G}^{ind}_{\infty}(\Omega,\vec{R},k_z,\omega)$ is the Fourier transform of $\overleftrightarrow{G}^{ind}_{\infty}$ with respect to z. For both expressions, $\overleftrightarrow{G}^{ind}$ denotes the induced part of the Green tensor, which is obtained from the Green tensor by subtracting the free-space contribution.

The advantage of the formalism given by eqs 5 to 8 is twofold. First, these expressions are universal. In particular, they can be used in conjunction with any modal decomposition of the Green tensor. We will consider one simple example in the following section. Second, these expressions clearly point out the fact that generally EELS can be related to the z-LDOS, while CL can be related to the z-rLDOS. Precisely, EELS and CL can be viewed respectively as probing generalized full and radiative densities of states that are local in real space along the $\vec{R}$ direction and in momentum space along the z direction, as was well established for EELS and the full EMLDOS only.[15,17]

We note an additional free-space contribution within the full and radiative EMLDOS compared to EELS and CL, which is due to the fact that contrary to a dipole a fast electron in a vacuum does not lose any energy. While this term leads to some minor differences between EMLDOS and fast electron based spectroscopies, we will consider exclusively the induced part of the Green tensor to focus on the resemblance between the z-LDOS and EELS as opposed to the resemblance between the z-rLDOS and CL.

MODAL DECOMPOSITIONS

In order to illustrate the consequences of the link between EELS (CL) and full EMLDOS (radiative EMLDOS) on their spatial and spectral variations, we now turn to deriving modal decompositions. Contrary to the textbook case of a non-absorbing and nondispersive closed system,[2] the link between the Green tensor and the eigenmodes is not straightforward for an arbitrary system. In the following, we consider a small metallic object of dielectric function $\epsilon(\omega)$, in such a way that the quasistatic approximation can be applied close to the object (in the near field). For small objects, the main energy loss mechanism is the excitation of SP modes, whose oscillations can give rise to light emission. We note that introducing the quasistatic approximation leads to a very slight violation of the energy conservation principle, as the full energy transfer is equal to the energy absorbed by the object without any contribution from the energy transferred into the far field. However, it allows defining rather easily SP modes for arbitrary geometries that, as pure surface charge density waves, have a very intuitive nature.

In a BEM formalism, the SP modes of the object can be defined through the electric fields $\vec{E}_i(\vec{r})$ obtained from a biorthogonal basis of geometric eigenmodes that only depend on the shape of the object.[9,28−30]

Besides a contribution that does not depend on the object geometry and gives rise to bulk energy losses, $\overleftrightarrow{G}^{ind}$ contains a surface term that can be expanded in the eigenmode basis.[30] Thanks to the biorthogonal character of this basis, this expansion reduces to a simple single summation over the modes. For simplicity, we consider in the following that the object is surrounded by vacuum. If $\vec{r}$ and $\vec{r}'$ are located outside the object, $\overleftrightarrow{G}^{ind}$ then reduces to the surface term and reads[30]

$$\overleftrightarrow{G}^{ind}(\vec{r},\vec{r}',\omega) = -\frac{1}{4\pi\omega^2}\sum_i f_i(\omega)\,\vec{E}_i(\vec{r})\otimes\vec{E}_i^*(\vec{r}') \quad (9)$$

where $f_i(\omega)$ is given by

$$f_i(\omega) = \frac{\lambda_i+1}{\lambda_i-\lambda(\omega)} \quad (10)$$

In this expression, λ_i is a real eigenvalue. $f_i(\omega)$ can be viewed as a spectral function characteristic of mode i.[29] The spectral weight of mode i in the decomposition is dominant at the energy $\hbar\omega$ that satisfies[29,30]

$$\lambda(\omega) = \frac{1+\epsilon(\omega)}{1-\epsilon(\omega)} \quad (11)$$

The advantage of the above set of equations relies on the fact that it explicitly depends on the object dielectric function without imposing any model. Therefore, any resonance line shape directly related to the optical properties of the metal can be reproduced.

The modal decomposition of eq 10 can be used directly to express the spatial and spectral variations of the full and radiative EMLDOS as well as EELS and CL through eqs 5 to 8. Because the object has very small dimensions compared to the radiation wavelength, one can show that the induced part of the far-field asymptote of the Green tensor satisfies:

$$\overleftrightarrow{G}^{ind}_{\infty}(\Omega,\vec{r}',\omega)\vec{e}_n = -\frac{1}{4\pi c^2}\sum_i f_i(\omega)\,E_i^{n*}(\vec{r}')\vec{p}_{i\perp}(\Omega) \quad (12)$$

where $\vec{p}_{i\perp}(\Omega) = \vec{p}_i - \vec{e}_r\cdot\vec{p}_i\vec{e}_r$ is the transverse component of the dipole moment $\vec{p}_i$ associated with the surface charge distribution of mode i.[24] We find that the contributions of $\overleftrightarrow{G}^{ind}$ to the n-LDOS and n-rLDOS can be written, if $\vec{r}_0$ is located in vacuum, as

$$\rho_n^{ind}(\vec{r}_0,\omega_0) = \frac{1}{2\pi^2\omega_0}\sum_i \Im\{f_i(\omega_0)\}|E_i^n(\vec{r}_0)|^2 \quad (13)$$

$$\rho_n^{rad,ind}(\vec{r}_0,\omega_0) = \frac{\omega_0^2}{8\pi^3c^3}\times\sum_i\sum_j f_i(\omega_0)f_j^*(\omega_0)\int_{4\pi}d\Omega\vec{p}_{i\perp}(\Omega)\cdot\vec{p}_{j\perp}^*(\Omega)\,E_i^{n*}(\vec{r}_0)\,E_j^n(\vec{r}_0) = \frac{\omega_0^2}{3\pi^2c^3}\sum_i|f_i(\omega_0)|^2|\vec{p}_i|^2|E_i^n(\vec{r}_0)|^2 + \frac{\omega_0^2}{4\pi^3c^3}\times\sum_i\sum_{j<i}\Re\{f_i(\omega_0)f_j^*(\omega_0)\int_{4\pi}d\Omega\vec{p}_{i\perp}(\Omega)\cdot\vec{p}_{j\perp}^*(\Omega)\,E_i^{n*}(\vec{r}_0)\,E_j^n(\vec{r}_0)\} \quad (14)$$

Furthermore, EELS and CL can be written, assuming that the electron travels exclusively in vacuum, as

DOI: 10.1021/acsphotonics.5b00416
ACS Photonics 2015, 2, 1619−1627

$$\Gamma^{\mathrm{EELS}}(\vec{R},\omega)=\frac{e^2}{\pi\hbar\omega^2}\sum_i \Im\{f_i(\omega)\}\left|\hat{E}_i^{z}(\vec{R},\omega/v)\right|^2 \tag{15}$$

$$\begin{aligned}\Gamma^{\mathrm{CL}}(\vec{R},\omega)&=\frac{e^2\omega}{4\pi^2\hbar c^3}\\&\times\sum_i\sum_j f_i(\omega)f_j^*(\omega)\int_{\Omega_D}\mathrm{d}\Omega\vec{p}_{i\perp}(\Omega)\cdot\vec{p}_{j\perp}^*(\Omega)\\&\hat{E}_i^{z*}(\vec{R},\omega/v)\,\hat{E}_j^{z}(\vec{R},\omega/v)\\&=\frac{e^2\omega}{4\pi^2\hbar c^3}\\&\times\sum_i|f_i(\omega)|^2\int_{\Omega_D}\mathrm{d}\Omega|\vec{p}_{i\perp}(\Omega)|^2|\hat{E}_i^{z}(\vec{R},\omega/v)|^2\\&+\frac{e^2\omega}{2\pi^2\hbar c^3}\\&\times\sum_i\sum_{j<i}\Re\{f_i(\omega)f_j^*(\omega)\int_{\Omega_D}d\Omega\vec{p}_{i\perp}(\Omega)\cdot\vec{p}_{j\perp}^*(\Omega)\,\hat{E}_i^{z*}(\vec{R},\omega/v)\\&\hat{E}_j^{z}(\vec{R},\omega/v)\}\end{aligned} \tag{16}$$

In the above expressions, $E_i^n(\vec{r})$ and $\hat{E}_i^z(\vec{R},k_z)$ respectively denote the projection along $\vec{e}_n$ of the electric field of mode i and the projection along z of the Fourier transform along z of the electric field of mode i. In the case of the full EMLDOS and EELS, we find the expressions given in ref 30, while the expression for the radiative EMLDOS is new and the one for CL is an extension of an approximate expression valid for non-overlapping modes published recently.[24]

GENERAL DISCUSSION

In this section, we discuss generally the modal decompositions given in eqs 13 to 16. Despite their similar spatial dependences, several consequences of the different character of the full EMLDOS (EELS) compared with the radiative EMLDOS (CL) can be viewed in the above decompositions. First, contrary to the full EMLDOS and EELS, the weight of each mode within the radiative EMLDOS and CL depends on its dipole moment. In particular, nondipolar modes contribute to both the full EMLDOS and EELS, while being absent from the radiative EMLDOS and CL. Moreover, the full EMLDOS and EELS are written as simple incoherent sums of modes, while the expressions for the radiative EMLDOS and CL include additional intermode coupled terms. These terms are non-vanishing when two dipolar modes overlap spatially through their electric fields and spectrally through their response functions $f_i(\omega)$ provided that their dipole moments are nonorthogonal. Except for these coupled terms, the spectral variations of CL and the radiative EMLDOS are related to the squared moduli of $f_i(\omega)$, while the spectral variations of EELS and the full EMLDOS are related to the imaginary parts of $f_i(\omega)$.

To comment in more simple terms on these spectral variations, we further consider the special case of a metallic object whose dielectric function is described by a Drude model $\varepsilon(\omega)=1-\omega_p^2/(\omega^2+i\Gamma\omega)$ (ω_p being the bulk plasmon energy and Γ a damping term). Although this model is too simplistic to accurately describe any real material, it allows obtaining simple analytical expressions that capture well the essence of the differences between full EMLDOS (EELS) and radiative EMLDOS (CL) close to metallic objects. Introducing the expression for the dielectric function within eq 11, one finds that the spectral function of mode i can be written

$$f_i(\omega)=\frac{\tilde{\omega}_i^2}{\tilde{\omega}_i^2-\omega^2-i\Gamma\omega}\approx\frac{\tilde{\omega}_i^2}{2\omega(\tilde{\omega}_i-\omega-i\Gamma/2)} \tag{17}$$

where $\tilde{\omega}_i=\sqrt{1+\lambda_i}\omega_p/\sqrt{2}$). It follows that the contributions of mode i to the spectral variations of EELS (full EMLDOS) and, in the absence of any intermode coupled term, CL (radiative EMLDOS) are respectively proportional to

$$\omega^{-3}\Im\{f_i(\omega)\}\approx\frac{\Gamma\tilde{\omega}_i^2}{4\omega^4[(\tilde{\omega}_i-\omega)^2+\Gamma^2/4]} \tag{18}$$

and

$$|f_i(\omega)|^2\approx\frac{\tilde{\omega}_i^4}{4\omega^2[(\tilde{\omega}_i-\omega)^2+\Gamma^2/4]} \tag{19}$$

Within a Drude model, the spectral variations of EELS (full EMLDOS) and, in the absence of any intermode coupled term, CL (radiative EMLDOS) are given by the Lorentzian line shapes given by eqs 18 and 19. Due to the ω^{-2} factor between $\omega^{-3}\Im\{f_i(\omega)\}$ and $|f_i(\omega)|^2$, spectral shifts increasing with dissipation are expected between the EELS (full EMLDOS) and CL (radiative EMLDOS) resonances associated with a single mode.[24] Such spectral shifts have been experimentally measured recently.[24] Furthermore, the CL and radiative EMLDOS resonances may be affected by the intermode coupled terms, which can lead to asymmetric line shapes, while the EELS and full EMLDOS resonances remain Lorentzian. Previously, asymmetric CL line shapes as opposed to symmetric EELS line shapes have been pinpointed as Fano resonances in calculations on nanowires.[32] Our analysis shows that these asymmetric line shapes are due to interferences between the far-field radiation from locally excited modes, which cancel out in the full energy transfers due to additional absorption contributions.

It is also worth commenting on the magnitude of the modes in the decompositions with the help of the Drude model. By definition, radiative modes belong to both the radiative and full EMLDOS, while nonradiative modes belong to the full EMLDOS only. The radiative character of a mode can further be quantified by its relative weight within the radiative EMLDOS, which can be inferred from the radiative EMLDOS to full EMLDOS ratio at resonance for a fixed position. At the resonance of mode i, one finds that the radiative EMLDOS to full EMLDOS ratio is proportional to $\tilde{\omega}_i^4|\vec{p}_i|^2$. Similarly, the CL to EELS ratio at the resonance of mode i is proportional to $\tilde{\omega}_i^4\int_{\Omega_D}\mathrm{d}\Omega|\vec{p}_{i\perp}(\Omega)|^2$ and can thus be taken as an equally valuable quantification of the radiative character of the mode. The relative weight of a mode within the radiative EMLDOS (CL) increases with the dipole moment and the resonance energy of the mode. Therefore, both the ability of the mode to efficiently scatter light into the far field through its dipole moment and the spectral range where its resonance energy falls are taken into account within its radiative weight. In a Drude model, the radiative weight of a mode increases with energy because absorption losses decrease with increasing energy.

We note that our analysis leads to the conclusion that no Fano-like interference can be detected in EELS for small metallic objects, as opposed to the conclusion of Collins et al.,[32] who proposed to interpret some intensity reinforcement along nanowires as the result of some mode interferences. However, our model is in accordance with their observations that CL

DOI: 10.1021/acsphotonics.5b00416
ACS Photonics 2015, 2, 1619−1627

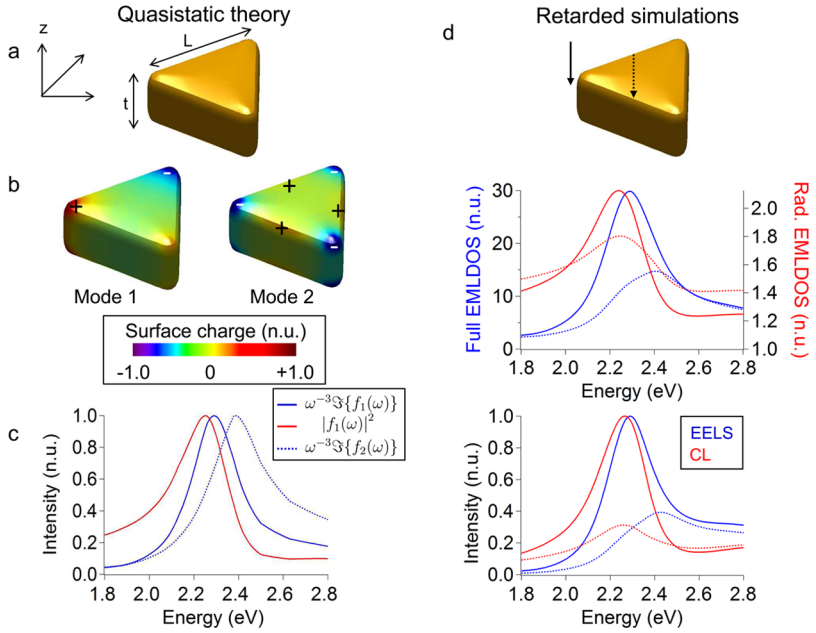

Figure 1. Full and radiative EMLDOS, and EELS and CL, close to a small gold triangular nanoprism. (a–c) Results obtained from the quasistatic theory. (a) Sketch of the nanoprism with length L = 40 nm and thickness t = 20 nm. (b) Surface charges of a dipolar (mode 1) and hexapolar mode (mode 2). (c) Spectral weight of mode 1 (blue continuous line) and mode 2 (blue dashed line) within the full EMLDOS/EELS and of mode 1 within the radiative EMLDOS/CL (red line). (d) Results obtained from retarded simulations: z-projected EMLDOS (upper graph) and EELS and CL (lower graph) spectra close to the tip (solid lines) and side (dotted lines) of a similar nanoprism. The full and radiative EMLDOS are normalized to the vacuum EMLDOS. EELS and CL are normalized to their respective maxima.

resonances can be asymmetric as opposed to EELS and that the spatial distributions of EELS and CL associated with a given mode are the same. Nevertheless, our decompositions cannot predict the complicated EELS and CL line shapes calculated by Bigelow and co-workers in more complex bimetallic structures with nonconnex geometry,[33] whose Green tensor spectral variations cannot be accounted for by the simple spectral function given in eq 11.

In general, the Green tensor of single metallic objects may be affected by the dielectric properties of the surrounding medium.[30] It can also be altered by retardation as the object size grows. Retardation effects in EELS and CL include the emission of transition radiation or Cherenkov radiation in dielectrics.[10] As another simple example, which will be illustrated in the next section, CL can probe some radiative modes with vanishing dipole moment for objects whose sizes leave the quasistatic regime. Indeed, the absence of any higher order mode in the radiative EMLDOS and CL is just due to the fact that the dimensions of the object are very small compared to the radiation wavelength. The absence of any higher order mode in the radiative EMLDOS and CL can be avoided by using alternative, retarded Green tensor expansions. The simplest example one can use is a phenomenological expansion for photonic eigenmodes accounting for weak losses[2] (see Supporting Information). However, such expansion is suitable to describe qualitatively the spectral behavior of the EMLDOS and fast electron based spectroscopies only in the simplest cases. As an example, such a model predicts a red-shift of EELS compared to CL, as opposed to the red-shift of CL compared to EELS measured in small gold objects in the visible range.[24]

NUMERICAL SIMULATIONS

In order to illustrate the discussion from the last section, we report the results obtained from BEM numerical simulations on concrete cases of metallic objects. We first examine two examples of small particles, in such a way that the quasistatic theory can be safely applied and tested, before turning to larger objects to investigate examples beyond the quasistatic limit.

As a first example, we consider a small gold equilateral triangular nanoprism, whose shape and dimensions are specified in Figure 1a. It has been shown that the EELS spectra of triangular nanoprisms are dominated by two degenerate dipolar modes and one hexapolar mode.[34] Figure 1b shows the surface charge associated with one of the dipolar modes (mode 1) and the hexapolar mode (mode 2). Because the two dipolar modes are degenerate, they contribute equally to the spectral variations of each modal decomposition without any interference effect. Mode 2 being nondipolar, the spectral variations of the radiative EMLDOS and CL are thus fully given by the term $|f_1(\omega)|^2$ (for mode 1). In comparison, the spectral variations of the full EMLDOS and EELS are dictated by both $\omega^{-3}\Im\{f_1(\omega)\}$ (mode 1) and $\omega^{-3}\Im\{f_2(\omega)\}$ (mode 2). These three quantities are plotted as a function of energy in Figure 1c when using a realistic tabulated dielectric function for gold.[35] As clear from these spectra, the resonance of $|f_1(\omega)|^2$ appears to be red-shifted compared to the resonance of $\omega^{-3}\Im\{f_1(\omega)\}$. These findings provided by the quasistatic theory are checked with retarded numerical simulations by calculating z-projected EMLDOS (upper graph) and EELS and CL (lower graph of Figure 1d) spectra close to the tip (solid lines) and side (dotted lines) of a similar nanoprism. Close to the tip, the spectra are dominated by the contribution from the dipolar modes,[34] and the radiative EMLDOS and CL resonances are respectively red-shifted compared to the full EMLDOS and EELS resonances. This red-shift reflects the absorption properties of gold in the visible range.[24] Close to the side, a higher energy resonance is found only in the full EMLDOS and EELS, showing that the

DOI: 10.1021/acsphotonics.5b00416
ACS Photonics 2015, 2, 1619–1627

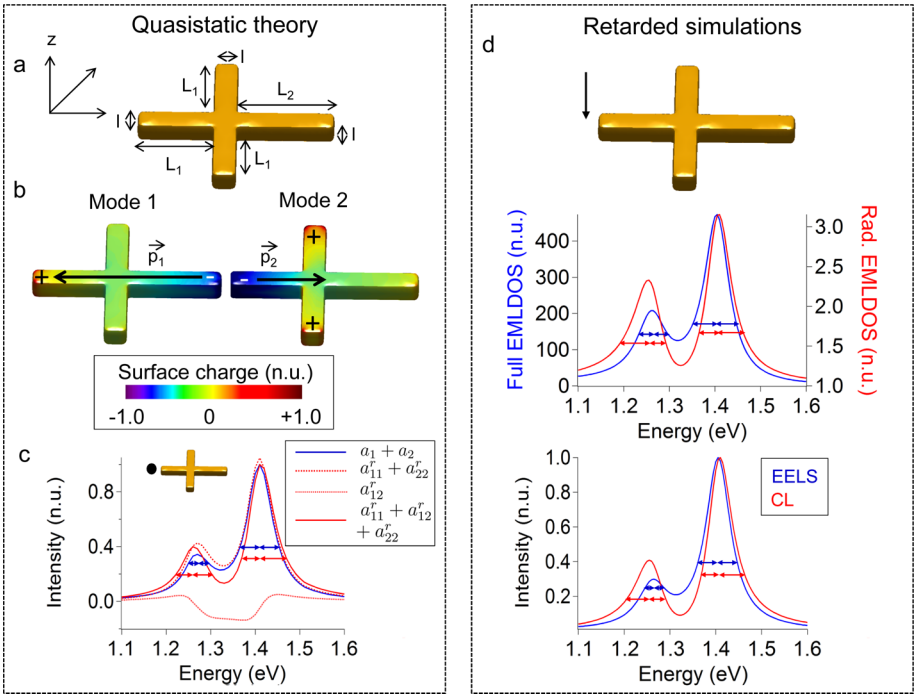

Figure 2. Full and radiative EMLDOS, and EELS and CL, close to a small gold asymmetric nanocross. (a–c) Results obtained from the quasistatic theory. (a) Sketch of the nanocross with dimensions L_1 = 17.5 nm, L_2 = 22.5 nm, and l = 5 nm. (b) Surface charges of the two lowest order modes. $\vec{p}_1$ and $\vec{p}_2$ represent their dipole moments. (c) Spectral weights of modes 1 and 2 within the z-projected full EMLDOS (blue line) and the z-projected radiative EMLDOS (red lines). The expressions for the different terms involved are $a_1 = \omega^{-3}\Im\{f_1(\omega)\}|E_1^z(\vec{r})|^2$, $a_2 = \omega^{-3}\Im\{f_2(\omega)\}|E_2^z(\vec{r})|^2$, $a_{11}^r = |f_1(\omega)|^2|\vec{p}_1|^2|E_1^z(\vec{r})|^2$, $a_{22}^r = |f_2(\omega)|^2|\vec{p}_2|^2|E_2^z(\vec{r})|^2$, and $a_{12}^r = 2\Re\{f_1(\omega)\, f_2^*(\omega)\vec{p}_1\cdot\vec{p}_2^*\, E_1^{z*}(\vec{r})\, E_2^z(\vec{r})\}$. These quantities are calculated for a position close to the left end of the same nanocross. The blue and red arrows respectively emphasize the symmetric and asymmetric character of the resonances. (d) Results obtained from retarded simulations. z-Projected EMLDOS (upper spectra) and EELS and CL (lower spectra) close to the left end of the same nanocross. The full and radiative EMLDOS are normalized to the vacuum EMLDOS. EELS and CL are normalized to their respective maxima. The blue and red arrows emphasize the symmetric (respectively asymmetric) character of the resonances in the full EMLDOS and EELS (respectively radiative EMLDOS and CL).

hexapolar mode belongs only to the full EMLDOS and can be probed only with EELS.

As a second example, we examine a small asymmetric gold nanocross (Figure 2a). Such an object supports two dipolar SP modes with parallel dipole moments $\vec{p}_1$ and $\vec{p}_2$, whose surface charges are shown in Figure 2b. In this case, an interference term contributes to the modal decompositions of the radiative EMLDOS and CL. In order to evaluate its contribution in the case of the radiative EMLDOS, we plot in Figure 2c the noninterfering terms involving separately modes 1 and 2, the coupled term involving both modes 1 and 2, and the resulting sum as a function of energy. We also compare this sum to its full EMLDOS counterpart. The coupled term is slightly positive below the first resonance and above the second resonance, while being largely negative between the two resonances. It leads to an asymmetric line shape when added to the two other terms, which are symmetric in comparison. On the contrary, the line shape of the full EMLDOS remains symmetric. Although the modal decompositions involve slightly different terms, these findings remain obviously true for EELS and CL. We compare the predictions from the quasistatic theory to retarded simulations by calculating z-projected EMLDOS (upper spectra) and EELS and CL (lower spectra of Figure 2d) spectra close to the left end of a similar nanocross. The radiative EMLDOS and CL spectra clearly show asymmetric line shapes, contrary to the full EMLDOS and EELS spectra. Furthermore, the CL to EELS and radiative EMLDOS to full EMLDOS ratios are higher around the resonance of mode 1 than around the resonance of mode 2. This is in agreement with both the facts that mode 1 has a dipole moment larger than mode 2 and that absorption losses increase with energy in gold due to interband transitions.

Finally, we perform retarded simulations for long silver nanowires. For lengths greater than around 100 nm, high-order longitudinal modes can be probed both in EELS[22,32,36−38] and in CL.[12,21,32,38,39] Figure 3 shows calculations of the z-projected full and radiative EMLDOS as well as EELS and CL along the axis of a 400 nm long silver wire. The qualitative agreement between EELS and z-LDOS on one hand and CL and z-rLDOS on the other is obvious from the plots. While EELS and the full EMLDOS clearly show high-order longitudinal multipolar modes up to m = 8, CL and the radiative EMLDOS show multipoles up to m = 4 only. In accordance with previous works,[21,32,38−40] we note that both the radiative EMLDOS and CL signal decrease monotonically when the order of the mode is increased. In particular, modes with zero dipole moment (e.g., m = 2, 4), which cannot be excited by light with normal incidence, are efficiently detected in CL. This makes an important distinction between the radiative modes, which belong to the radiative EMLDOS and are probed by CL, and the modes usually denoted as dark in the literature.[41,42] Furthermore, the radiative EMLDOS (CL) to full EMLDOS (EELS) ratio decreases when the order of the mode is increased.[38,40] This trend reflects the reduced radiative

DOI: 10.1021/acsphotonics.5b00416
ACS Photonics 2015, 2, 1619−1627

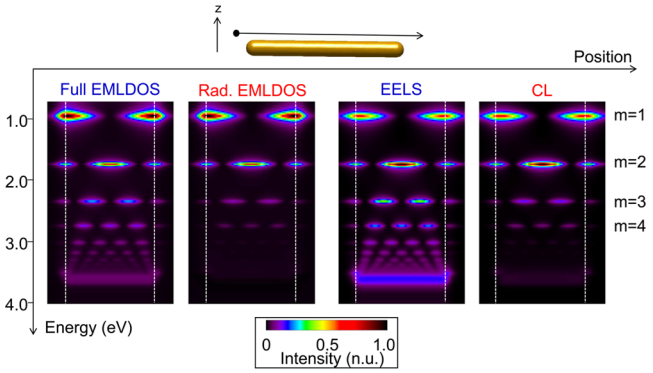

Figure 3. z-Projected full and radiative EMLDOS, and EELS and CL, calculated close to a 400 nm long silver nanowire with a diameter of 40 nm. The four quantities are normalized to their respective maxima. The dashed white lines symbolize the particle edges. The four first resonances, corresponding to longitudinal multipolar modes, are denoted as $m = 1$ to 4.

character of the multipolar modes, which is due to both the increase of absorption losses at higher energies and the reduction of radiative damping when the multipolar order of the mode is increased.[38,43] Lastly, Figure 4 compares EELS and

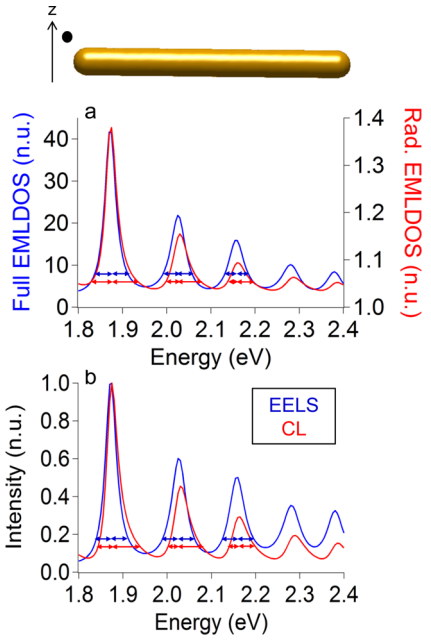

Figure 4. z-Projected full and radiative EMLDOS (a) and EELS and CL spectra (b) calculated close to the end of a 2 μm long, 40 nm thick silver nanowire. The blue and red arrows emphasize the symmetric (respectively asymmetric) character of the resonances in the full EMLDOS and EELS (respectively radiative EMLDOS and CL).

CL spectra (b) to z-projected full and radiative EMLDOS spectra (a) in the case of a 2 μm long wire. Such wires exhibit asymmetric CL resonances as opposed to symmetric EELS resonances.[32] Similarly, the radiative EMLDOS shows asymmetric line shapes contrary to the full EMLDOS. These simple examples illustrate perfectly the link between EELS (CL) and z-LDOS (z-rLDOS) beyond the quasistatic limit.

CONCLUSION

In this article, we have established a clear link between EELS and the projection along the electron direction of the full EMLDOS on one hand and CL and the projection along the electron direction of the radiative EMLDOS on the other. Starting from a unified formalism based on the use of the Green tensor, we have analyzed modal decompositions of the full EMLDOS, the radiative EMLDOS, EELS, and CL in order to clarify this relationship. Besides probing the radiative modes only, CL and the radiative EMLDOS can show different spectral line shapes affected by intermode interferences due to energy transfer into the far field. These conclusions are supported by retarded numerical simulations.

This work demonstrates that EELS and CL are advantageous techniques to locally probe projected full and radiative EMLDOS over a broad spectral range. As the radiative character of a mode may be invaluable information, most particularly in complex systems,[44−46] the understanding of SP modes should highly benefit from combined EELS and CL experiments. More generally, accessing both the radiative and full EMLDOS would be desirable in order to efficiently tailor light−matter interaction at the nanoscale. To go further, the relation between EELS and the Green tensor combined with modal decompositions has been shown to be a key ingredient for a full three-dimensional reconstruction of the EMLDOS out of EELS data.[47] Our extension to CL should be used appropriately, owing to the recently reported possibility of CL tomography,[48] which follows EELS tomography.[49]

Eventually, although any mode definition remains delicate in arbitrary absorbing systems, we note that a retarded mode expansion of the Green tensor has been proposed.[50] The present work calls for the derivation and analysis of modal decompositions in a framework including retardation.

METHODS

Green Tensor Definitions. In this article, we make use of the electric Green tensor of a polarizable system described by a space- and frequency-dependent dielectric function $\epsilon(\vec{r}, \omega)$. It is defined in Gaussian units by the equation:[15]

$$\vec{\nabla} \times \vec{\nabla} \times \overleftrightarrow{G}(\vec{r}, \vec{r}', \omega) - \frac{\omega^2}{c^2}\epsilon(\vec{r}, \omega)\, \overleftrightarrow{G}(\vec{r}, \vec{r}', \omega) = -\frac{1}{c^2}\delta(\vec{r} - \vec{r}') \tag{20}$$

and is taken to satisfy the vacuum Sommerfeld radiation boundary condition at infinity. The electric field induced by an arbitrary external current density distribution $\vec{J}_{ext}(\vec{r}, \omega)$ can then be expressed as[15]

$$\vec{E}(\vec{r}, \omega) = -4\pi i\omega \int \mathrm{d}\vec{r}'\, \overleftrightarrow{G}(\vec{r}, \vec{r}', \omega)\, \vec{J}_{ext}(\vec{r}', \omega) \tag{21}$$

Next,[10] we introduce the far-field amplitude $\vec{f}(\Omega, \omega)$, from which the far-field limit of the electric field can be written as

$$\vec{E}(\vec{r}, \omega) \xrightarrow[\omega r/c \to \infty]{} \frac{e^{i\omega r/c}}{r}\vec{f}(\Omega, \omega) \tag{22}$$

where Ω denotes the direction of $\vec{r}$. Direct identification between eqs 22 and 21 allows introducing the far-field asymptotic Green tensor $\overleftrightarrow{G}_\infty(\Omega, \vec{r}', \omega) = re^{-i\omega r/c} \lim_{\omega r/c \to \infty} \overleftrightarrow{G}(\vec{r}, \vec{r}', \omega)$ as the $\omega r/c \to \infty$ limit of the solution of eq 20. The far-field amplitude can be

DOI: 10.1021/acsphotonics.5b00416
ACS Photonics 2015, 2, 1619−1627

expressed as a function of the far-field asymptotic Green tensor as

$$\vec{f}\,(\Omega, \omega) = -4\pi i\omega \int \mathrm{d}\vec{r}'\, \vec{\vec{G}}_{\infty}(\Omega, \vec{r}', \omega)\, \vec{J}_{\mathrm{ext}}(\vec{r}', \omega) \quad (23)$$

General Definitions and Derivation. The projections along the unit vector $\vec{e}_n$ of the full and radiative EMLDOS are defined following their usual classical interpretation.[2] Precisely, the full EMLDOS at position $\vec{r}_0$ and energy $\hbar\omega_0$ is proportional to the time-averaged power transferred from an electric dipole point source of dipole moment $\vec{p}_0$ located at position $\vec{r}_0$ and oscillating at frequency ω_0 to its environment. Furthermore, the radiative EMLDOS at position $\vec{r}_0$ and energy $\hbar\omega_0$ is proportional to the power transferred from the same point source to the far field. Multiplying the expressions in Gaussian units[31] by a prefactor $1/\pi^2|\vec{p}_0|^2\omega_0{}^2$ leads to eqs 1 and 2, in which $\vec{E}_d(\vec{r}, \omega)$ and $f_d(\Omega, \omega)$ are solutions of eqs 21 and 23 with $\vec{J}_{\mathrm{ext}}(\vec{r}, \omega) = -i\omega\vec{p}_0\delta(\vec{r} - \vec{r}_0)\,\delta(\omega - \omega_0)$. Introducing the Green tensor through eqs 21 and 23 together with the expression for the electric dipole current density further leads to eqs 5 and 6.

Similarly, EELS and CL are respectively obtained from the force exerted by the electric field induced by and acting back on a fast electron and from the energy collected in the far field. This definition of CL assumes purely coherent light emission processes.[10] After Fourier decomposition, the energy loss and light emission probabilities can be expressed, for a given electron trajectory $\vec{r}_e(t)$ and a given energy $\hbar\omega$, as eqs 3 and 4.[10] In these expressions, $\vec{E}_{\mathrm{el}}^{\mathrm{ind}}(\vec{r}, \omega)$ and $\vec{f}_{\mathrm{el}}^{\mathrm{ind}}(\Omega, \omega)$ are obtained from the solutions of eqs 21 and 23, with $\vec{J}_{\mathrm{ext}}(\vec{r}, \omega) = -e\vec{v}\int \mathrm{d}t\, \mathrm{e}^{i\omega t}\,\delta(\vec{r} - \vec{r}_e(t))$, by removing the free-space solution. Further assuming an electron trajectory with a constant velocity $\vec{v}$ directed along z, we obtain eqs 7 and 8, where $\overleftrightarrow{G}^{\mathrm{ind}}(\vec{R}, \vec{R}, k_z, k_z', \omega)$ is the

$$= \iint \mathrm{d}z\mathrm{d}z' \mathrm{e}^{i(k_z z + k_z' z')} \vec{\vec{G}}^{\mathrm{ind}}(\vec{R} + z\vec{e}_z, \vec{R} + z'\vec{e}_z, \omega)$$

Fourier transform of $\vec{\vec{G}}^{\mathrm{ind}}$ with respect to z and z' and $\overleftrightarrow{G}_{\infty}^{\mathrm{ind}}(\Omega, \vec{R}, k_z, \omega) = \int \mathrm{d}z\, \mathrm{e}^{ik_z z} \vec{\vec{G}}_{\infty}^{\mathrm{ind}}(\Omega, \vec{R} + z\vec{e}_z, \omega)$ is the Fourier transform of $\vec{\vec{G}}_{\infty}^{\mathrm{ind}}$ with respect to z.

Numerical Simulations. Numerical simulations are performed using the MNPBEM toolbox.[26,27] Quasistatic eigenmodes are calculated numerically using the quasistatic eigenmode solver. EMLDOS, EELS, and CL spectra are computed using the retarded solver in combination with the dipole and fast electron excitation classes. For simplicity, the CL spectra are computed along a 4π solid angle. The dielectric function of gold and silver are obtained from ref 35.

■ ASSOCIATED CONTENT

Supporting Information

The Supporting Information is available free of charge on the ACS Publications website at DOI: 10.1021/acsphotonics.5b00416.

Phenomenological retarded modal decompositions (PDF)

■ AUTHOR INFORMATION

Corresponding Author

*E-mail: arthur.losquin@fysik.lth.se.

Notes

The authors declare no competing financial interest.

■ ACKNOWLEDGMENTS

The authors acknowledge Prof. F. J. García de Abajo for fruitful discussions. The research leading to these results has received funding from the European Union Seventh Framework Programme [No. FP7/2007-2013] under Grant Agreement No. n312483 (ESTEEM2).

■ REFERENCES

(1) Novotny, L.; Hecht, B. *Principles of Nano-Optics*; Cambridge University Press, 2011.

(2) Carminati, R.; Cazé, A.; Cao, D.; Peragut, F.; Krachmalnicoff, V.; Pierrat, R.; De Wilde, Y. Electromagnetic density of states in complex plasmonic systems. *Surf. Sci. Rep.* **2015**, *70*, 1−41.

(3) Joulain, K.; Carminati, R.; Mulet, J.-P.; Greffet, J.-J. Definition and measurement of the local density of electromagnetic states close to an interface. *Phys. Rev. B: Condens. Matter Mater. Phys.* **2003**, *68*, 245405.

(4) Joulain, K.; Mulet, J.-P.; Marquier, F.; Carminati, R.; Greffet, J.-J. Surface electromagnetic waves thermally excited: Radiative heat transfer, coherence properties and Casimir forces revisited in the near field. *Surf. Sci. Rep.* **2005**, *57*, 59.

(5) Weeber, J.-C.; Dereux, A.; Girard, C.; Krenn, J. R.; Goudonnet, J.-P. Plasmon polaritons of metallic nanowires for controlling submicron propagation of light. *Phys. Rev. B: Condens. Matter Mater. Phys.* **1999**, *60*, 9061.

(6) De Wilde, Y.; Formanek, F.; Carminati, R.; Gralak, B.; Lemoine, P.-A.; Joulain, K.; Mulet, J.-P.; Chen, Y.; Greffet, J.-J. Thermal radiation scanning tunnelling microscopy. *Nature* **2006**, *444*, 740.

(7) Colas Des Francs, G.; Girard, C.; Bruyant, A.; Dereux, A. SNOM signal near plasmonic nanostructures: an analogy with fluorescence decays channels. *J. Microsc.* **2008**, *229*, 302−306.

(8) Cao, D.; Cazé, A.; Calabrese, M.; Pierrat, R.; Bardou, N.; Collin, S.; Carminati, R.; Krachmalnicoff, V.; De Wilde, Y. Mapping the Radiative and the Apparent Nonradiative Local Density of States in the Near Field of a Metallic Nanoantenna. *ACS Photonics* **2015**, *2*, 189−193.

(9) Kociak, M.; Stéphan, O. Mapping plasmons at the nanometer scale in an electron microscope. *Chem. Soc. Rev.* **2014**, *43*, 3865.

(10) de Abajo, F. J. G. Optical excitations in electron microscopy. *Rev. Mod. Phys.* **2010**, *82*, 209−275.

(11) Yamamoto, N.; Araya, K.; García de Abajo, F. Photon emission from silver particles induced by a high-energy electron beam. *Phys. Rev. B: Condens. Matter Mater. Phys.* **2001**, *64*, 205419.

(12) Vesseur, E. J. R.; de Waele, R.; Kuttge, M.; Polman, A. Direct Observation of Plasmonic Modes in Au Nanowires Using High-Resolution Cathodoluminescence Spectroscopy. *Nano Lett.* **2007**, *7*, 2843.

(13) Bosman, M.; Keast, V. J.; Watanabe, M.; Maaroof, A. I.; Cortie, M. B. Mapping surface plasmons at the nanometre scale with an electron beam. *Nanotechnology* **2007**, *18*, 165505.

(14) Nelayah, J.; Kociak, M.; Stéphan, O.; García de Abajo, F. J.; Tencé, M.; Henrard, L.; Taverna, D.; Pastoriza-Santos, I.; Liz-Marzán, L. M.; Colliex, C. Mapping surface plasmons on a single metallic nanoparticle. *Nat. Phys.* **2007**, *3*, 348.

(15) García de Abajo, F. J.; Kociak, M. Probing the Photonic Local Density of States with Electron Energy Loss Spectroscopy. *Phys. Rev. Lett.* **2008**, *100*, 106804.

(16) Kuttge, M.; Vesseur, E. J. R.; Koenderink, A. F.; Lezec, H. J.; Atwater, H. A.; García de Abajo, F. J.; Polman, A. Local density of states, spectrum, and far-field interference of surface plasmon polaritons probed by cathodoluminescence. *Phys. Rev. B: Condens. Matter Mater. Phys.* **2009**, *79*, 113405.

(17) Hohenester, U.; Ditlbacher, H.; Krenn, J. R. Electron-Energy-Loss Spectra of Plasmonic Nanoparticles. *Phys. Rev. Lett.* **2009**, *103*, 106801.

DOI: 10.1021/acsphotonics.5b00416
ACS Photonics 2015, 2, 1619−1627

(18) Vesseur, E. J. R.; García de Abajo, F. J.; Polman, A. Modal Decomposition of Surface Plasmon Whispering Gallery Resonators. *Nano Lett.* **2009**, *9*, 3147.
(19) Barnard, E. S.; Coenen, T.; Vesseur, E. J. R.; Polman, A.; Brongersma, M. L. Imaging the Hidden Modes of Ultrathin Plasmonic Strip Antennas by Cathodoluminescence. *Nano Lett.* **2011**, *11*, 4265.
(20) Sapienza, R.; Coenen, T.; Renger, J.; Kuttge, M.; van Hulst, N. F.; Polman, A. Deep-subwavelength imaging of the modal dispersion of light. *Nat. Mater.* **2012**, *11*, 781−787.
(21) Gómez-Medina, R.; Yamamoto, N.; Nakano, M.; García de Abajo, F. J. Mapping plasmons in nanoantennas via cathodoluminescence. *New J. Phys.* **2008**, *10*, 105009.
(22) Rossouw, D.; Couillard, M.; Vickery, J.; Kumacheva, E.; Botton, G. A. Multipolar Plasmonic Resonances in Silver Nanowire Antennas Imaged with a Subnanometer Electron Probe. *Nano Lett.* **2011**, *11*, 1499.
(23) García de Abajo, F. Relativistic energy loss and induced photon emission in the interaction of a dielectric sphere with an external electron beam. *Phys. Rev. B: Condens. Matter Mater. Phys.* **1999***59*, 3095.10.1103/PhysRevB.59.3095
(24) Losquin, A.; Zagonel, L. F.; Myroshnychenko, V.; Rodríguez-González, B.; Tencé, M.; Scarabelli, L.; Förstner, J.; Liz-Marzán, L. M.; García de Abajo, F. J.; Stéphan, O.; Kociak, M. Unveiling Nanometer Scale Extinction and Scattering Phenomena through Combined Electron Energy Loss Spectroscopy and Cathodoluminescence Measurements. *Nano Lett.* **2015**, *15*, 1229−1237.
(25) García de Abajo, F. J.; Howie, A. Retarded field calculation of electron energy loss in inhomogeneous dielectrics. *Phys. Rev. B: Condens. Matter Mater. Phys.* **2002**, *65*, 115418.
(26) Hohenester, U.; Trugler, A. MNPBEM A Matlab toolbox for the simulation of plasmonic nanoparticles. *Comput. Phys. Commun.* **2012**, *183*, 370.
(27) Hohenester, U. Simulating electron energy loss spectroscopy with the {MNPBEM} toolbox. *Comput. Phys. Commun.* **2014**, *185*, 1177−1187.
(28) Ouyang, F.; Isaacson, M. Surface plasmon excitation of objects with arbitrary shape and dielectric constant. *Philos. Mag. B* **1989**, *60*, 481.
(29) García de Abajo, F. J.; Aizpurua, J. Numerical simulation of electron energy loss near inhomogeneous dielectrics. *Phys. Rev. B: Condens. Matter Mater. Phys.* **1997**, *56*, 15873.
(30) Boudarham, G.; Kociak, M. Modal decompositions of the local electromagnetic density of states and spatially resolved electron energy loss probability in terms of geometric modes. *Phys. Rev. B: Condens. Matter Mater. Phys.* **2012**, *85*, 245447.
(31) Jackson, J. D. *Classical Electrodynamics*, 2nd ed.; Wiley: New York, 1975.
(32) Collins, S. M.; Nicoletti, O.; Rossouw, D.; Ostasevicius, T.; Midgley, P. A. Excitation dependent Fano-like interference effects in plasmonic silver nanorods. *Phys. Rev. B: Condens. Matter Mater. Phys.* **2014**, *90*, 155419.
(33) Bigelow, N. W.; Vaschillo, A.; Camden, J. P.; Masiello, D. J. Signatures of Fano Interferences in the Electron Energy Loss Spectroscopy and Cathodoluminescence of Symmetry-Broken Nanorod Dimers. *ACS Nano* **2013**, *7*, 4511−4519.
(34) Schmidt, F. P.; Ditlbacher, H.; Hofer, F.; Krenn, J. R.; Hohenester, U. Morphing a Plasmonic Nanodisk into a Nanotriangle. *Nano Lett.* **2014**, *14*, 4810−4815.
(35) Johnson, P. B.; Christy, R. W. Optical Constants of the Noble Metals. *Phys. Rev. B* **1972**, *6*, 4370−4379.
(36) Nicoletti, O.; Wubs, M.; Mortensen, N. A.; Sigle, W.; van Aken, P. A.; Midgley, P. A. Surface plasmon modes of a single silver nanorod: an electron energy loss study. *Opt. Express* **2011**, *19*, 15371−15379.
(37) Schoen, D. T.; Atre, A. C.; García-Etxarri, A.; Dionne, J. A.; Brongersma, M. L. Probing Complex Reflection Coefficients in One-Dimensional Surface Plasmon Polariton Waveguides and Cavities Using STEM EELS. *Nano Lett.* **2015**, *15*, 120−126.
(38) Martin, J.; Kociak, M.; Mahfoud, Z.; Proust, J.; Gérard, D.; Plain, J. High-Resolution Imaging and Spectroscopy of Multipolar Plasmonic Resonances in Aluminum Nanoantennas. *Nano Lett.* **2014**, *14*, 5517−5523.
(39) Arbouet, A.; Mlayah, A.; Girard, C.; des Francs, G. C. Electron energy losses and cathodoluminescence from complex plasmonic nanostructures: spectra, maps and radiation patterns from a generalized field propagator. *New J. Phys.* **2014**, *16*, 113012.
(40) Taminiau, T. H.; Stefani, F. D.; van Hulst, N. F. Optical Nanorod Antennas Modeled as Cavities for Dipolar Emitters: Evolution of Sub- and Super-Radiant Modes. *Nano Lett.* **2011**, *11*, 1020−1024.
(41) Chu, M.-W.; Myroshnychenko, V.; Chen, C. H.; Deng, J.-P.; Mou, C.-Y.; de Abajo, F. J. G. Probing Bright and Dark Surface-Plasmon Modes in Individual and Coupled Noble Metal Nanoparticles Using an Electron Beam. *Nano Lett.* **2009**, *9*, 399−404.
(42) Neubrech, F.; Garcia-Etxarri, A.; Weber, D.; Bochterle, J.; Shen, H.; Lamy de la Chapelle, M.; Bryant, G. W.; Aizpurua, J.; Pucci, A. Defect-induced activation of symmetry forbidden infrared resonances in individual metallic nanorods. *Appl. Phys. Lett.* **2010**, *96*, 213111.
(43) Zhang, S.; Chen, L.; Huang, Y.; Xu, H. Reduced linewidth multipolar plasmon resonances in metal nanorods and related applications. *Nanoscale* **2013**, *5*, 6985−6991.
(44) Stockman, M. I.; Faleev, S. V.; Bergman, D. J. Localization versus Delocalization of Surface Plasmons in Nanosystems: Can One State Have Both Characteristics? *Phys. Rev. Lett.* **2001**, *87*, 167401.
(45) Bosman, M.; Anstis, G. R.; Keast, V. J.; Clarke, J. D.; Cortie, M. B. Light Splitting in Nanoporous Gold and Silver. *ACS Nano* **2012**, *6*, 319−326.
(46) Losquin, A.; Camelio, S.; Rossouw, D.; Besbes, M.; Pailloux, F.; Babonneau, D.; Botton, G. A.; Greffet, J.-J.; Stéphan, O.; Kociak, M. Experimental evidence of nanometer-scale confinement of plasmonic eigenmodes responsible for hot spots in random metallic films. *Phys. Rev. B: Condens. Matter Mater. Phys.* **2013**, *88*, 115427.
(47) Hoerl, A.; Trügler, A.; Hohenester, U. Full three-dimensonal reconstruction of the dyadic Green tensor from electron energy loss spectroscopy of plasmonic nanoparticles. *ACS Photonics* **2015**.
(48) Atre, A. C.; Brenny, B. J.; Coenen, T.; García-Etxarri, A.; Polman, A.; Dionne, J. A. Nanoscale optical tomography with cathodoluminescence spectroscopy. *Nat. Nanotechnol.* **2015**, *10*, 429.
(49) Nicoletti, O.; de La Peña, F.; Leary, R. K.; Holland, D. J.; Ducati, C.; Midgley, P. A. Three-dimensional imaging of localized surface plasmon resonances of metal nanoparticles. *Nature* **2013**, *502*, 80−84.
(50) Sauvan, C.; Hugonin, J. P.; Carminati, R.; Lalanne, P. Modal representation of spatial coherence in dissipative and resonant photonic systems. *Phys. Rev. A: At., Mol., Opt. Phys.* **2014**, *89*, 043825.

DOI: 10.1021/acsphotonics.5b00416
ACS Photonics 2015, 2, 1619−1627